Three-dimensional imaging of intraplaque neovascularization in a mouse model of advanced atherosclerosis

Perrotta, P.; Pintelon, I.; Vries, M.R. de; Quax, P.H.A.; Timmermans, J.P.; Meyer, G.R.Y. de; Martinet, W.

JVR
Journal of
Vascular Research

Methods in Vascular Biology

J Vasc Res 2020;57:348–354
DOI: 10.1159/000508449

Received: March 31, 2020
Accepted: May 6, 2020
Published online: July 1, 2020

Three-Dimensional Imaging of Intraplaque Neovascularization in a Mouse Model of Advanced Atherosclerosis

Paola Perrotta[a] Isabel Pintelon[b] Margreet R. de Vries[c, d] Paul H.A. Quax[c, d]
Jean-Pierre Timmermans[b] Guido R.Y. De Meyer[a] Wim Martinet[a]

[a]Laboratory of Physiopharmacology, University of Antwerp, Antwerp, Belgium; [b]Laboratory of Cell Biology and Histology, University of Antwerp, Antwerp, Belgium; [c]Department of Surgery, Leiden University Medical Center, Leiden, The Netherlands; [d]Einthoven Laboratory for Experimental Vascular Medicine, Leiden University Medical Center, Leiden, The Netherlands

Keywords
Immunolabeling-enabled three-dimensional imaging of solvent-cleared organs · Intraplaque angiogenesis · Atherosclerosis

Abstract
Multiple lines of evidence suggest that intraplaque (IP) neovascularization promotes atherosclerotic plaque growth, destabilization, and rupture. However, pharmacological inhibition of IP neovascularization remains largely unexplored due to the limited number of animal models that develop IP neovessels and the lack of reliable methods for visualizing IP angiogenesis. Here, we applied 3D confocal microscopy with an optimized tissue-clearing process, immunolabeling-enabled three-dimensional imaging of solvent-cleared organs, to visualize IP neovessels in apolipoprotein E-deficient ($ApoE^{-/-}$) mice carrying a heterozygous mutation (C1039+/–) in the fibrillin-1 gene. Unlike regular $ApoE^{-/-}$ mice, this mouse model is characterized by the presence of advanced plaques with evident IP neovascularization. Plaques were stained with antibodies against endothelial marker CD31 for 3 days, followed by incubation with fluorescently labeled secondary antibodies. Subsequent tissue clearing with dichloromethane (DCM)/methanol, DCM, and dibenzyl ether allowed easy visualization and 3D reconstruction of the IP vascular network while plaque morphology remained intact.

Introduction

Atherosclerosis is a progressive inflammatory disease that leads to plaque formation at specific sites of the arterial tree [1]. Formation of atherosclerotic plaques typically starts with the deposition of lipids in the intima, followed by endothelial activation and infiltration of macrophages and other inflammatory cells into the subendothelial layer. The first grossly visible vascular lesions, called fatty streaks, transform into more advanced lesions by the migration and proliferation of vascular smooth muscle cells, activation of macrophages, and the accumulation of lipid-rich necrotic debris. These plaques typically have a thick fibrous cap consisting of vascular smooth muscle cells and extracellular matrix that encloses a lipid-rich necrotic core [2, 3]. Over time, plaques can

karger@karger.com
www.karger.com/jvr

Wim Martinet
Laboratory of Physiopharmacology
University of Antwerp
Universiteitsplein 1, BE–2610 Antwerp (Belgium)
wim.martinet@uantwerpen.be

become increasingly complex with calcification, ulceration at the luminal surface, and the presence of small neovessels that grow into the lesion from the media of the blood vessel wall. Several stimuli inside the plaque such as hypoxia and high oxidative stress trigger the formation of such intraplaque (IP) neovessels [4]. Growing evidence suggests that IP neovessels are leaky and promote the entry of several plaque components including RBCs, lipids, and inflammatory cells [5], which may accelerate the progression and destabilization of developing plaques [6, 7]. Along these lines, blocking IP angiogenesis has been proposed as a novel approach for decreasing plaque instability and for limiting cardiovascular risk [8, 9]. Apolipoprotein E-deficient ($ApoE^{-/-}$) mice containing a heterozygous mutation (C1039G+/–) in the fibrillin-1 (Fbn1) gene represent a unique mouse model of advanced atherosclerosis with human-like plaque characteristics such as IP neovascularization [10, 11]. Unlike other experimental models of atherosclerosis, $ApoE^{-/-}Fbn1^{C1039G+/-}$ mice show fragmentation of elastic fibers, which facilitates neovessel sprouting from the adventitial vasa vasorum into the plaque [12], similarly to what occurs in human plaques. Conventional immunohistochemistry is currently the gold standard for analysis of plaque composition, yet it does not allow an accurate visualization and quantification of such neovessels inside the complex structure of the plaque. In the present study, we optimized an optical ex vivo clearing method for the visualization of IP angiogenesis in $ApoE^{-/-}Fbn1^{C1039G+/-}$ mice, termed immunolabeling-enabled three-dimensional imaging of solvent-cleared organs (iDISCO).

Materials and Methods

Mice

Female $ApoE^{-/-}Fbn1^{C1039G+/-}$ mice were fed a Western-type diet (WD) (Altromin, C1000 diet supplemented with 20% milk fat and 0.15% cholesterol, #100171) starting at 8 weeks of age. After 20 weeks on the WD, mice were euthanized with an overdose of sodium pentobarbital (250 mg/kg i.p.) and perfused with 20 mL of 4% paraformaldehyde (PFA) in PBS. Carotid arteries were dissected and incubated in 4% PFA in PBS overnight. Standard $ApoE^{-/-}$ mice that did not contain the C1039+/– mutation (but fed WD for 20 weeks) were used as negative controls since they develop plaques without IP neovascularization. All animal procedures were conducted according to the guidelines from Directive 2010/63/EU of the European Parliament on the protection of animals used for scientific purposes. Experiments were approved by the ethics committee of the University of Antwerp.

Immunostaining and iDISCO Clearing

Tissue samples were incubated in permeabilization solution (1 × PBS, 0.2% Triton X-100, 0.3 M glycine, and 20% DMSO) overnight. Samples were then washed for 1 h in 1 × PBS/0.2% Tween-20 and incubated in blocking buffer (1 × PBS, 0.2% Triton X-100, 10% DMSO, and 3% donkey serum) for 8 h, followed by incubation with primary rat anti-mouse CD31 antibody (Abcam, ab56299; 10 μg/mL) in permeabilization buffer (1 × PBS, 0.2% Triton X-100, 0.3 M glycine, and 20% DMSO) for 72 h. Finally, samples were washed 3 times in 1 × PBS and 0.2% Triton X-100 followed by incubation with goat anti-rat Alexa Fluor 546 (Thermo Fisher, A11081; 1:500 dilution) for 48 h. For nuclear labeling, the samples were incubated with DAPI (Sigma-Aldrich, 5 μg/mL) for 30 min. Next, immunolabeled samples were dehydrated in a methanol (MeOH) gradient (in PBS) by incubating tissue specimens in 20% MeOH (30 min), 50% MeOH (30 min), 70% MeOH (30 min), and 100% MeOH (overnight). Subsequently, the samples were incubated for 2 h in 66% dichloromethane (DCM)/34% MeOH, and then washed twice for 15 min in 100% DCM. Finally, the samples were incubated in dibenzyl ether (DBE) until transparency was achieved (approximately 3 h).

Confocal Imaging and Histology

Cleared samples were imaged on an inverted Leica TCS SP8 confocal laser scanning microscope, using a 20×/0.75 HC PL Apo objective lens. The samples were positioned in a glass-bottom Petri dish and submerged in DBE. DAPI was visualized using a 405-nm diode laser, and the Alexa Fluor 546 fluorescence was imaged with the 546-nm wavelength of a white light laser. For each sample, an image stack (z step size ~5 μm) with 1,024 × 1,024 pixel resolution was captured. Three-dimensional renderings were obtained using Leica LAS X 3D visualization software. The Imaris image analysis software enabled the specific selection and measurement of the IP blood vessels, by applying a new surface rendering based on the intensity of the fluorescent signal. Following the imaging, the samples were embedded in paraffin, cut into 5-μm sections, and stained with hematoxylin and eosin (H&E). H&E stains were imaged using an Olympus BX43 microscope.

Results and Discussion

We previously reported that the heterozygous mutation C1039G+/– in the Fbn1 gene leads to advanced unstable atherosclerotic plaques in $ApoE^{-/-}$ mice, a standard mouse model of atherosclerosis [10, 11]. Fbn1 is an extracellular matrix glycoprotein secreted by fibroblasts and incorporated into microfibrils. These fibrillin-rich microfibrils are associated with cross-linked elastin to form mature elastic fibers. Mutations in the Fbn1 gene result in impaired microfibrillar assembly and deposition, followed by fragmentation of elastic fibers. This loss of structural integrity of the vessel wall leads to progressive dilatation and arterial stiffening, resembling vascular aging [11]. Fragmentation of the elastic fibers gives rise to elastin-derived peptides, which attract monocytes, en-

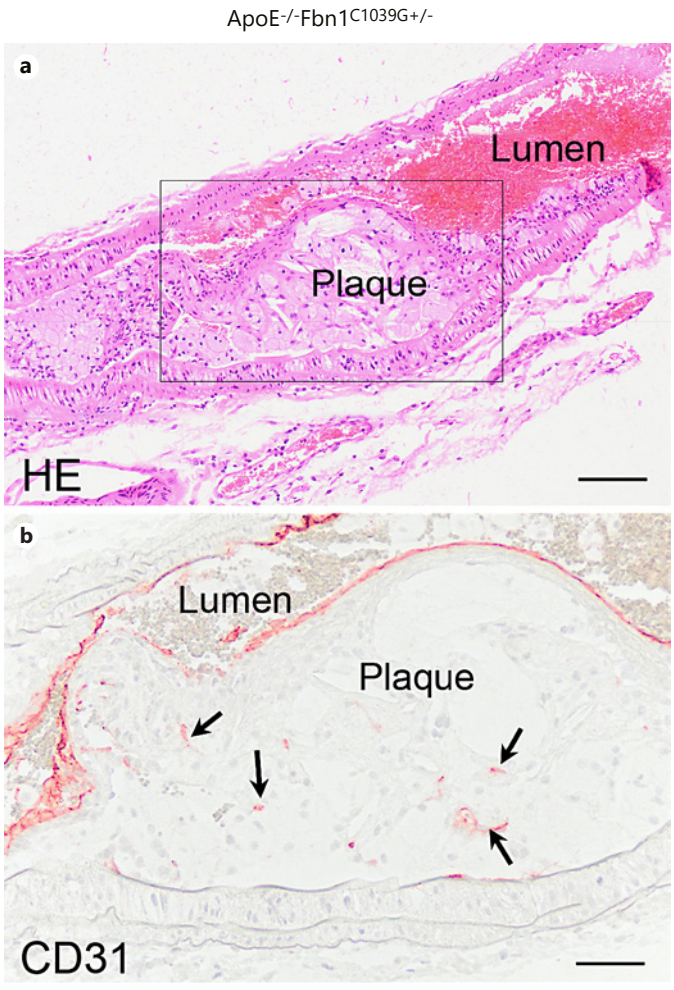

Fig. 1. Standard (immuno)histochemical analyses of IP neovascularization in carotid artery plaques (arrows) from ApoE$^{-/-}$Fbn1$^{C1039G+/-}$ mice that were fed a Western diet for 20 weeks. **a** Representative low- power micrograph of an H&E-stained, paraffin-embedded longitudinal section of carotid plaque. Scale bar, 100 µm. **b** Detail of plaque with intraplaque microvessel stain for CD31 (boxed area in panel **a**) Scale bar, 50 µm. IP, intraplaque; H&E, hematoxylin and eosin.

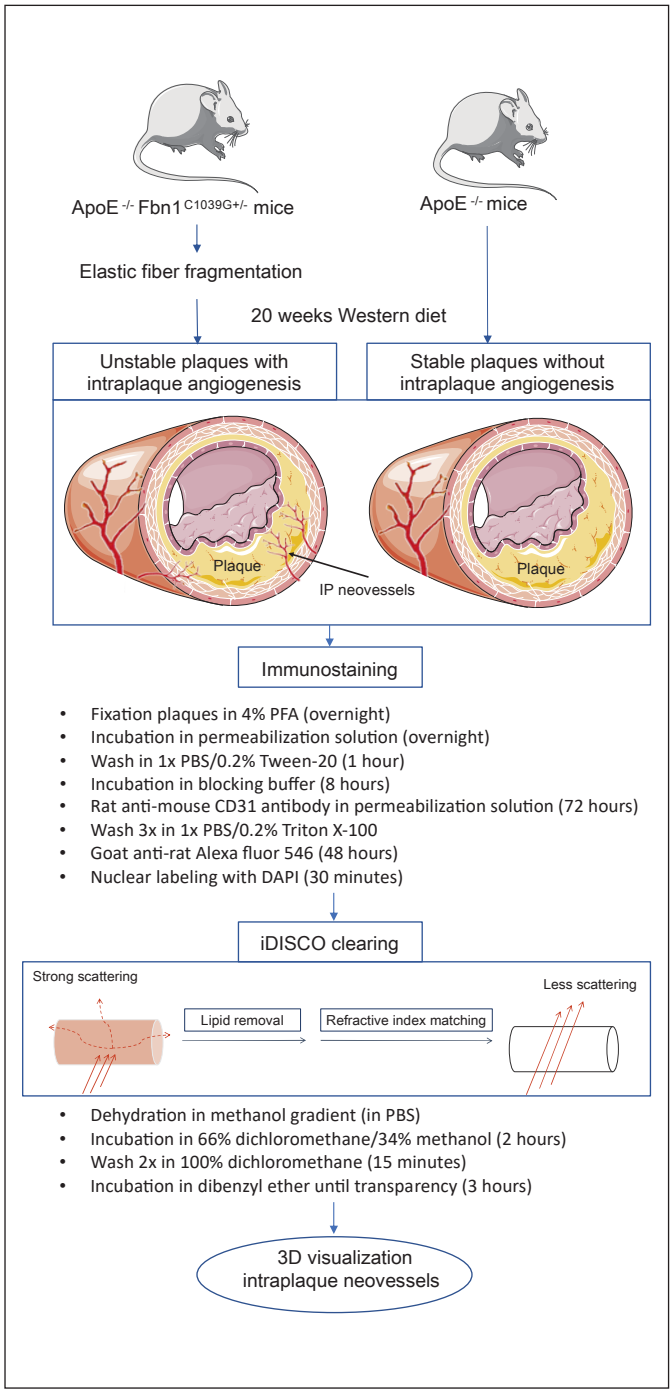

Fig. 2. Schematic overview of the different steps required for immunostaining and tissue clearing. Solvent-based tissue clearing is a three-step process. First, the tissue is dehydrated and lipids are removed by sequential incubation in a MeOH gradient (20, 50, 70, and 100% methanol in distilled water). Second, the tissue is transferred to a high refractive index solution where additional lipid solvation and clearing occur (66% DCM/34% methanol). Finally, the lipid-free tissue sample is placed in a high refractive index matching solution (DBE) for further clearing. DCM, dichloromethane; DBE, dibenzyl ether; MeOH, methanol.

hancing the inflammatory reaction in the vessel wall. Moreover, extensive neovascularization is observed in the brachiocephalic and common carotid arteries of ApoE$^{-/-}$Fbn1$^{C1039G+/-}$ mice fed the WD [12]. These features are rarely seen in murine atherosclerosis models but are frequently observed in advanced human plaques. IP neovessels in ApoE$^{-/-}$Fbn1$^{C1039G+/-}$ mice on the WD likely arise from the adventitial vasa vasorum and sprout out of the media into the plaque [9]. Although the exact role of IP neovessels is not exactly understood, it is important to note that such structures are immature and leaky. Indeed, besides being an entry point for leukocytes and li-

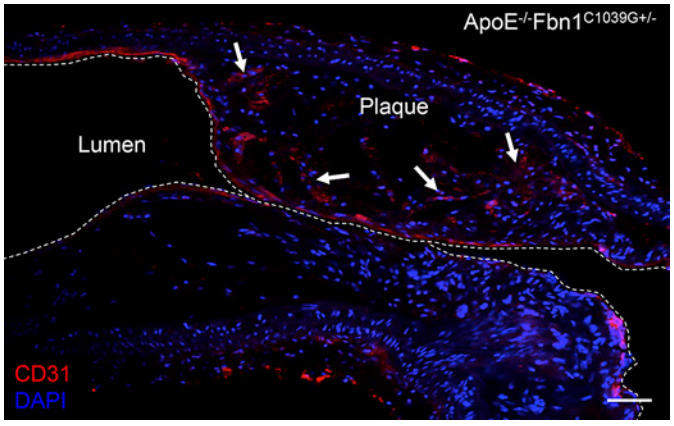

Fig. 3. Representative 2D visualization of IP neovascularization in a single z-stack slide of a carotid artery plaque from ApoE$^{-/-}$Fbn1$^{C1039G+/-}$ mice after CD31 immunohistochemical staining and iDISCO clearing. Multiple red-stained CD31-positive ECs are detectable inside the plaque (arrows). Scale bar, 50 μm. IP, intraplaque; iDISCO, immunolabeling-enabled three-dimensional imaging of solvent-cleared organs; EC, endothelial cell.

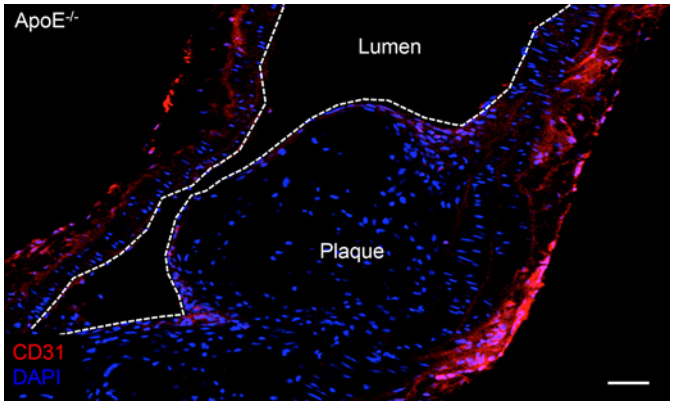

Fig. 4. IP neovascularization is absent in plaques of ApoE$^{-/-}$ mice. A single representative z-stack slide of a plaque in the brachiocephalic artery is shown. CD31-positive cells (red) are not present inside the plaque, but clearly detectable in the intima. Scale bar, 50 μm. IP, intraplaque.

poproteins, IP neovessels appear to be a source of erythrocytes and platelets inside the plaque, thereby promoting macrophage activation and plaque destabilization.

Imaging of IP neovascularization is possible in human plaques using microvascular imaging and contrast-enhanced ultrasonography [13–16], though this approach is not feasible (or at least unlikely) in mouse plaques due to the extremely small size of the IP neovessels. Hitherto, immunohistochemical analysis of paraffin-embedded sections remains the only method for evaluating IP angiogenesis in mouse plaques. Figure 1 shows representative (immuno)histochemical stains of IP neovessels in plaques of ApoE$^{-/-}$Fbn1$^{C1039G+/-}$ mice. Because both contrast-enhanced ultrasonography and histological analysis of plaques are 2D imaging techniques, they have limitations regarding the interpretation of the "architecture" of microvessel circuits in the atherosclerotic plaque. In recent years, a technique called "tissue clearing" has reemerged, offering an alternative approach for tissue sectioning. Nowadays, numerous protocols allow optical clearing and detailed 3D imaging of intact organs [17–22].

iDISCO combines immunolabeling of large tissue samples for volume imaging with 3D imaging of solvent-cleared organs [23]. iDISCO is an optical clearing method that makes biological samples more transparent ("cleared") (Fig. 2) and has been successfully used to image three-dimensional structures, including intact mouse organs such as the brain, kidney, intestine, eye, and even whole embryos [18, 22–25]. Recently, Becher et al. [26] applied the iDISCO technology for 3D profiling of atherosclerotic plaques and arterial remodeling after carotid artery ligation. We optimized iDISCO for mouse atherosclerotic tissue using endothelial cell-specific CD31 antibodies, and we show here for the first time a 3D reconstruction of IP neovascularization in carotid plaques of ApoE$^{-/-}$Fbn1$^{C1039G+/-}$ mice. From our experience, the following modifications to the iDISCO protocol were essential for obtaining good visualization of neovessels in carotid plaques: (1) high CD31 antibody concentrations (10 μg/mL) were required for best imaging results, (2) an overnight incubation step in permeabilizing solution for good tissue penetration of the primary antibody, though we recommend a 72-h incubation, and (3) a simple clearing protocol with a mixture of 66% DCM and 34% MeOH, followed by incubation in pure DCM, and DBE was sufficient to visualize the IP vascular network, in contrast to previously published protocols that are more labor-intensive [17].

Cleared samples of total organs are typically visualized using light sheet microscopy, allowing rapid 3D imaging of these large samples [17, 19–21]. Less thick, cleared specimens can also be imaged by confocal microscopy, and hence benefit from the higher resolution that can be obtained [22]. Imaging of cleared segments of the carotid arteries by confocal microscopy resulted in visualization of the delicate IP neovascularization in carotid plaques of ApoE$^{-/-}$Fbn1$^{C1039G+/-}$ mice and confirmed the labeling of IP neovessels and the complete clearing of the carotid artery segments.

Three-dimensional reconstruction (see online suppl. Video 1; see www.karger.com/doi/10.1159/000508449 for

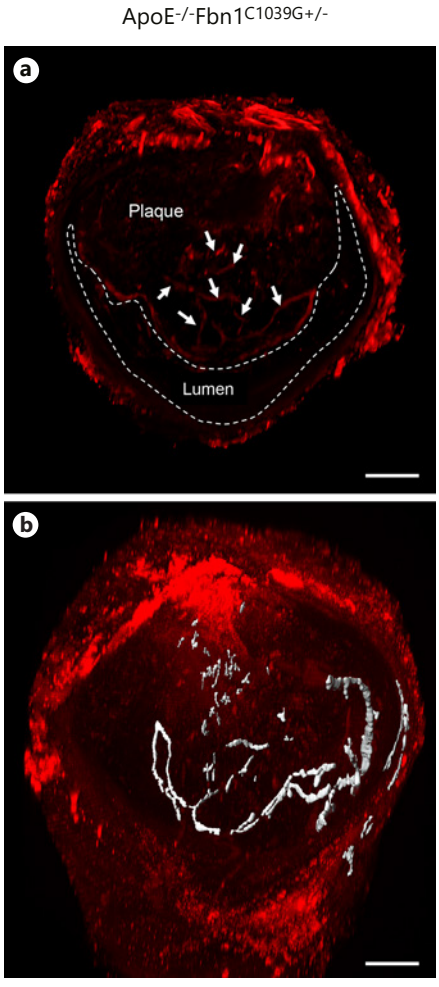

Fig. 5. Representative 3D reconstruction of a carotid artery segment (50 z-stack slides) from ApoE$^{-/-}$Fbn1$^{C1039G+/-}$ mice after CD31 immunohistochemical staining and iDISCO clearing. **a** Multiple red-stained CD31-positive ECs are detectable inside the plaque that is bulging the lumen. The 3D reconstruction clearly illustrates the complex distribution of the neovascularization inside the plaque (white arrows). **b** Using 3D analysis software, neovessels entering the plaque can selectively be depicted (gray) in the 3D image, and quantitative measurements such as the total of volume of the IP vessels can be obtained. Scale bar, 80 μm. IP, intraplaque; iDISCO, immunolabeling-enabled three-dimensional imaging of solvent-cleared organs; EC, endothelial cell.

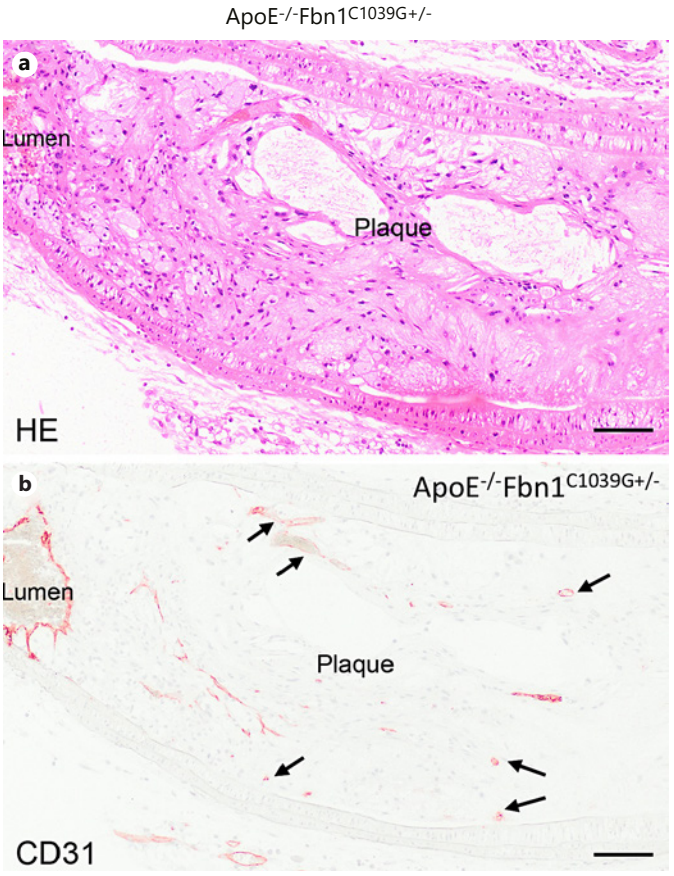

Fig. 6. a, **b** H&E staining and CD31 immunohistochemical staining of a carotid artery plaque from a representative ApoE$^{-/-}$Fbn1$^{C1039G+/-}$ mouse after iDISCO clearing, showing that the morphology of the plaque and the structure of the neovessels (arrows) were not affected by the clearing procedure. Scale bar, 100 μm. H&E, hematoxylin and eosin; iDISCO, immunolabeling-enabled three-dimensional imaging of solvent-cleared organs.

all online suppl. material) and a z-stack (online suppl. Video 2) show the high degree of tortuosity and irregularities in the structure of IP neovessels from ApoE$^{-/-}$Fbn1$^{C1039G+/-}$ mice, which is not obvious in single plane images of 2D sections (Fig. 3). To evaluate the specificity of endothelial CD31 staining in IP angiogenesis, we also applied this technique to regular ApoE$^{-/-}$ mice that develop plaques after being fed the WD, albeit without IP neovascularization. The recorded z-stack shows that CD31 staining did not occur in carotid plaques of ApoE$^{-/-}$ mice (online suppl. video 3), although it was clearly present at the luminal endothelial cell layer and in the adventitia (Fig. 4). Further analyses of the obtained images demonstrated that the applied technique is not only limited to the visualization of the 3D distribution of the IP neovascularization (Fig. 5a). Using 3D analysis software, neovessels entering the plaque can be selectively depicted in the 3D rendering, and quantitative measurements can be obtained (white area in Fig. 5b). The total volume of IP vessels as shown in Figure 5b was calculated to be 0.068 mm^3 and can be used to compare IP angiogenesis between different plaques. Clearing procedures such as 3D imaging of solvent-cleared organs lead to substantial shrinkage and

might affect tissue morphology [22, 27]. However, the shorter clearing procedure that was used for the carotid segments definitely protected the tissue from the effects of the clearing process, as the structure of the plaque was not altered after clearing. This was confirmed by applying our standard 2D histological techniques on the cleared tissues after imaging, allowing us to examine the structure and composition of the plaque (Fig. 6). Moreover, fluorescent labeling of the tissue was preserved after the clearing process and paraffin embedding (data not shown) allowing re-examination of H&E-stained sections of the paraffin-embedded tissue by fluorescence microscopy, if needed.

Clearing and 3D imaging of human artery segments were not performed in this study and might present certain challenges and constraints. Considering the thickness and composition of human plaques, we expect that the described iDISCO procedure for mouse tissue will need to be adapted and will become more complex with longer incubation times for dehydration and clearing. Because of their size, 3D imaging of human plaques will require dedicated light sheet microscopy. In addition to the clearing procedure limitations that have already been described by Ertürk et al. [27], such as that this protocol can only be used on fixed tissues and that samples cannot be stored for prolonged periods, the toxicity of the organic solutions used in our protocol might be an extra limitation. Nevertheless, our protocol is straightforward and reproducible, which makes it an effective method for visualizing and analyzing neovessels inside atherosclerotic plaques.

In conclusion, this is the first report to apply iDISCO technology to atherosclerotic blood vessels, and it provides a simple, inexpensive, and effective method for visualizing and reconstructing, in three dimensions, the presence of IP neovessels inside these lesions. This could be a useful new tool for studies aimed at determining whether there is a causal relationship between the presence of neovessel structures and atherogenesis or between angiogenic stimuli and plaque angiogenesis.

Acknowledgements

The authors would like to thank Rita Van den Bossche, Mandy Vermont, Dominique De Rijck, and Gleison D.P. Bossolani for technical help. The authors are grateful to Dr. Bronwen Martin for critical reading of the manuscript.

Statement of Ethics

All animal procedures were conducted according to the guidelines from Directive 2010/63/EU of the European Parliament on the protection of animals used for scientific purposes. Experiments were approved by the ethics committee of the University of Antwerp.

Conflict of Interest Statement

The authors have no conflicts of interest to declare.

Funding Sources

This work was supported by the University of Antwerp (DOCPRO-BOF) and the Horizon 2020 program of the European Union – Marie Sklodowska Curie actions – ITN – MOGLYNET [Grant No. 675527]. The Leica SP 8 (Hercules grant AUHA.15.12) confocal microscope was funded by the Hercules Foundation of the Flemish Government.

Author Contributions

Paola Perrotta, Isabel Pintelon, and Wim Martinet: study conception and design. Paola Perrotta, Isabel Pintelon, and Margreet R. de Vries: acquisition of data. All authors contributed to the analysis and interpretation of data. All authors also helped drafting the manuscript and approved the final version of the manuscript.

References

1 Ross R. Atherosclerosis is an inflammatory disease. Am Heart J. 1999 Nov;138(5 Pt 2): S419–20.
2 Moreno PR, Sanz J, Fuster V. Promoting mechanisms of vascular health: circulating progenitor cells, angiogenesis, and reverse cholesterol transport. J Am Coll Cardiol. 2009 Jun 23;53(25):2315–23.
3 Bentzon JF, Otsuka F, Virmani R, Falk E. Mechanisms of plaque formation and rupture. Circ Res. 2014 Jun 6;114(12):1852–66.
4 Moreno PR, Purushothaman KR, Sirol M, Levy AP, Fuster V. Neovascularization in human atherosclerosis. Circulation. 2006 May 9; 113(18):2245–52.
5 de Vries MR, Quax PH. Plaque angiogenesis and its relation to inflammation and atherosclerotic plaque destabilization. Curr Opin Lipidol. 2016 Oct;27(5):499–506.
6 Stary HC, Chandler AB, Dinsmore RE, Fuster V, Glagov S, Insull W Jr, et al. A definition of advanced types of atherosclerotic lesions and a histological classification of atherosclerosis. A report from the committee on vascular lesions of the council on arteriosclerosis, American heart association. Arterioscler Thromb Vasc Biol. 1995 Sep 1;15(9):1512–31.

7 Nakamura J, Nakamura T, Deyama J, Fujioka D, Kawabata K, Obata JE, et al. Assessment of carotid plaque neovascularization using quantitative analysis of contrast-enhanced ultrasound imaging is useful for risk stratification in patients with coronary artery disease. Int J Cardiol. 2015 Sep 15;195:113–9.
8 Parma L, Baganha F, Quax PHA, de Vries MR. Plaque angiogenesis and intraplaque hemorrhage in atherosclerosis. Eur J Pharmacol. 2017 Dec 5;816:107–15.
9 Perrotta P, Emini Veseli B, Van der Veken B, Roth L, Martinet W, De Meyer GRY. Pharmacological strategies to inhibit intra-plaque angiogenesis in atherosclerosis. Vascul Pharmacol. 2019 Jan;112:72–8.
10 Van Herck J, De Meyer G, Martinet W, Van Hove C, Foubert K, Theunis M, et al. Impaired fibrillin-1 function promotes features of plaque instability in apolipoprotein E-deficient mice. Circulation. 2009 Dec 15;120(24):2478–87.
11 Van der Donckt C, Van Herck JL, Schrijvers DM, Vanhoutte G, Verhoye M, Blockx I, et al. Elastin fragmentation in atherosclerotic mice leads to intraplaque neovascularization, plaque rupture, myocardial infarction, stroke, and sudden death. Eur Heart J. 2015 May 1;36(17):1049–58.
12 Emini Veseli B, Perrotta P, De Meyer GRA, Roth L, Van der Donckt C, Martinet W, et al. Animal models of atherosclerosis. Eur J Pharmacol. 2017 Dec 5;816:3–13.
13 Coli S, Magnoni M, Sangiorgi G, Marrocco-Trischitta MM, Melisurgo G, Mauriello A, et al. Contrast-enhanced ultrasound imaging of intraplaque neovascularization in carotid arteries: correlation with histology and plaque echogenicity. J Am Coll Cardiol. 2008 Jul 15;52(3):223–30.
14 Cattaneo M, Staub D, Porretta AP, Gallino JM, Santini P, Limoni C, et al. Contrast-enhanced ultrasound imaging of intraplaque neovascularization and its correlation to plaque echogenicity in human carotid arteries atherosclerosis. Int J Cardiol. 2016 Nov 15;223:917–22.
15 Andrews JPM, Fayad ZA, Dweck MR. New methods to image unstable atherosclerotic plaques. Atherosclerosis. 2018 May;272:118–28.
16 Oura K, Kato T, Ohba H, Terayama Y. Evaluation of intraplaque neovascularization using superb microvascular imaging and contrast-enhanced ultrasonography. J Stroke Cerebrovasc Dis. 2018 Sep;27(9):2348–53.
17 Richardson DS, Lichtman JW. Clarifying tissue clearing. Cell. 2015 Jul 16;162(2):246–57.
18 Vogt N. Transparency in large tissue samples. Nat Methods. 2015 Jan;12(1):11.
19 Ariel P. A beginner's guide to tissue clearing. Int J Biochem Cell Biol. 2017 Mar;84:35–9.
20 Richardson DS, Lichtman JW. Snapshot: tissue clearing. Cell. 2017 Oct 5;171(2):496–496.e1.
21 Orlich M, Kiefer F. A qualitative comparison of ten tissue clearing techniques. Histol Histopathol. 2018 Feb;33(2):11903–99.
22 GDP Bossolani, Pintelon I, Detrez JD, Buckinx R, Thys S, Zanoni JN, et al. Comparative analysis reveals Ce3D as optimal clearing method for in toto imaging of the mouse intestine. Neurogastroenterol Motil. 2019 May;31(5):e13560.
23 Renier N, Wu Z, Simon DJ, Yang J, Ariel P, Tessier-Lavigne M. iDISCO: a simple, rapid method to immunolabel large tissue samples for volume imaging. Cell. 2014 Nov 6;159(4):896–910.
24 Henning Y, Osadnik C, Malkemper EP. Eye-Ci: optical clearing and imaging of immunolabeled mouse eyes using light-sheet fluorescence microscopy. Exp Eye Res. 2019 Mar;180:137–45.
25 Walter A, van der Spek L, Hardy E, Bemelmans AP, Rouach N, Rancillac A. Structural and functional connections between the median and the ventrolateral preoptic nucleus. Brain Struct Funct. 2019 Dec;224(9):3045–57.
26 Becher T, Riascos-Bernal DF, Kramer DJ, Almonte V, Chi J, Tong T, et al. Three-dimensional imaging provides detailed atherosclerotic plaque morphology and reveals angiogenesis after carotid artery ligation. Circ Res. 2020 Feb;126(5):619–32.
27 Ertürk A, Becker K, Jährling N, Mauch CP, Hojer CD, Egen JG, et al. Three-dimensional imaging of solvent-cleared organs using 3DISCO. Nat Protoc. 2012 Nov;7(11):1983–95.